Design and deployment of a prototype multicomponent DAS sensor

Kris Innanen, Don Lawton, Kevin Hall, Kevin Bertram, Malcolm Bertram and Henry Bland

ABSTRACT

In 2016-2017 CREWES published a range of analyses and applications of a geometrical model of fibre-optic (DAS) data for arbitrary fibre shapes. Amongst those applications was a multicomponent estimation scheme based on a careful accounting, and combined useage, of the varying fibre directions associated with a shaped cable layout. In 2018 a prototype shaped DAS fibre array was buried to put some of these ideas and their feasibility to the test. In October 2018, "the pretzel" was illuminated from several directions, and shot records were analyzed to assess whether commonly available directional sensitivity is sufficient to permit multiple components of strain to be estimated simultaneously. By picking a P-wave arrival and comparing it to an analytic model, we conclude with a cautious yes. Other important directionality conclusions are also derivable from this experimental setup; for instance, a polarity ambiguity involving the DAS directionality modelling through accounting of local fibre tangents is clearly rendered when model and data are compared.

INTRODUCTION

In 2016-2017 CREWES published a geometric model to support analyses of the directionality properties of Distributed Acoustic Sensing (DAS) fibre-optic seismic systems (Innanen, 2017b; Eaid and Innanen, 2018; Eaid et al., 2018). One of the applications of the model was a framework for multicomponent sensing with shaped versions of either straight or helical-wound fibres (Innanen, 2017a). Within this framework, it was evident that given

1. Free rein to set up well-coupled DAS fibres in arbitrary shapes, and
2. Gauge lengths of order $\ll$ 1m,

the DAS signal at each of a relatively dense set of channel locations could be transformed into 6 traces, one for each independent component of strain or strain rate. However, current DAS interrogator technology, and the practicalities of field deployment, make assumptions (1) and (2) unrealistic. In 2018 CREWES set out to assess the practical possibility of multicomponent DAS sensing by designing and deploying a prototype sensor, in the form of a shaped loop of DAS fibre. Since it was to actually be buried, and field tested with an actual interrogator (with its gauge length / SNR restrictions), it was an opportunity to see how the approach of Innanen (2017a) managed given realistic limitations on (1)-(2).

The multi-directional DAS loop was surveyed and buried at the CaMI-FRS in Newell County Alberta. After roughly 1 month for the ground to settle, the loop was illuminated alongside surface 3C calibration phones. The partners in this were CaMI-FRS, Lawrence Berkeley National Labs (who supplied the helical-wound fibre), and Halliburton-Pinnacle, who supplied and operated the DAS interrogator hardware, and provided the resulting raw data. The purpose of this report is to describe this experiment, and to present early results and conclusions deriving from it.

Background

DAS technology applied to seismic sensing has ramped up dramatically in the last several years (Mestayer et al., 2011; Daley et al., 2013; Mateeva et al., 2013, 2014). Although not all of its original promise, especially in 4D sensing in deepwater wells (Chalenski et al., 2016), has been realized, the low cost of deployment has led to its use in many unconventional reservoir settings. Research and development both in academia and industry have been active in interrogator improvements, fibre hardware improvements (Yu et al., 2018; Willis et al., 2018), and in processing improvements (Hardeman-Vooys et al., 2018). Applications have also widened considerably (e.g., Huot et al., 2018).

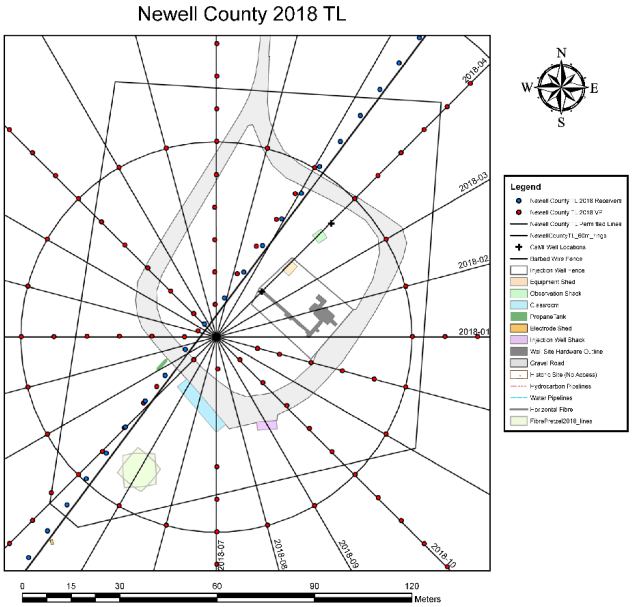

FIG. 1. CREWES 2018 walkaway-walkaround VSP shot map, detail near observation well (Hall et al., 2018). Southwest of the well the two overlain squares of the multicomponent DAS array can be seen in green.

DAS fibres respond proportionally to longitudinal strain or strain rate in the direction of the fibre axis only. This *directionality* has been a point of concern throughout the lifespan of the technology (e.g., Mateeva et al., 2014; Kuvshinov, 2016). Absent the complicating issue of ground-to-cladding-to-fibre coupling, the DAS measurement assigned to an output point can be thought of as projections of the point-wise tensor strain (or strain rate) onto a fibre along its local axial/tangential direction, followed by a weighted averaging over the gauge length centred on the output point. So, with reasonable accuracy, one can think of a DAS fibre as a "pointable" sensor, which will capture a portion of the strain tensor in whatever direction it is laid – provided the fibre interval so laid out exceeds the gauge length. Assuming this is so, multicomponent sensing, by virtue of a fibre which has been shaped to occupy a range of independent directions, becomes possible (Innanen, 2016, 2017a). This has been pointed elsewhere, but within a design paradigm permitting gauge lengths no larger than cm scale (Ning and Sava, 2018). The complex response of a very small-radius fibre wind, especially relative to its cladding, and the requirement for a cm-scale gauge length, means that such systems will require new hardware technology to appear before

they can be tested. Thus the possibility of a practical, deployable multicomponent DAS sensing array remains an open question.

DESIGN AND DEPLOYMENT

In collaboration with CaMI, a location nearby the FRS station trailer was selected for the prototype sensor to be deployed (Figure 1). Southwest of the observation well (identifiable as the centre of the star pattern), a twin-square shape is visible. This is the fibre array design in map view.

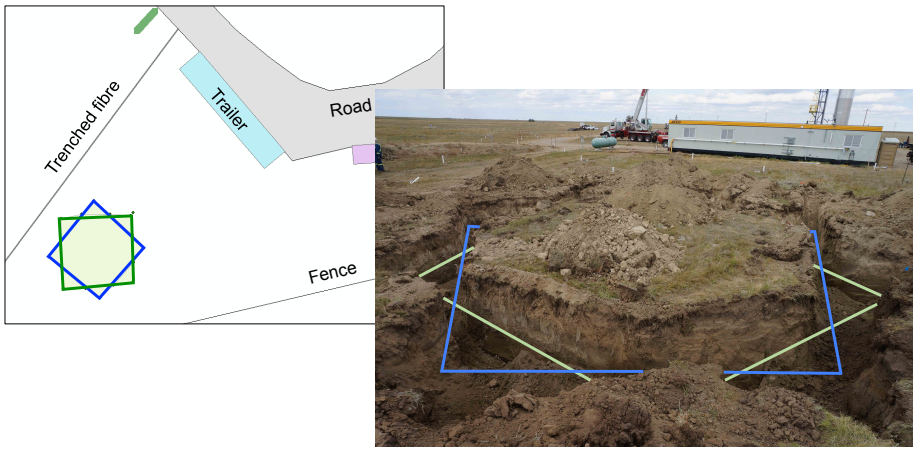

FIG. 2. Deployment detail in map (left) and photographic (right) view. The twin squares are distinguished with green and blue colours in all analysis to follow.

Optimal DAS responses occur, from experience (e.g., Hall et al., 2017), for fibres which have been deployed in boreholes, cemented behind casing; sensitivity issues may appear in trenched deployments. However, borehole environments are both expensive and bad for early-stage experimentation, since a drilling rig is needed, shapes are constrained to those which can be deployed regularly as casing goes in, and since you only get one shot to try anything. So, for practical purposes, our first try at a multicomponent DAS sensor was in a trenched and largely horizontal configuration.

The pattern of two squares with their repeated straight segments was chosen because it afforded good lateral directional coverage, and because it was straightforward to survey and excavate. In Figure 2 greater detail in plan view and a photograph of the excavation are shown. The two squares are distinguished schematically by the colours green and blue, with the edges of the green square approximately aligned with the cardinal directions and the edges of the blue square aligned with the NE-NW-SE-SW directions. A photograph of some of the detail of the fibre layout at the bottom of the 2m trench, and a diagram of the associated points on the array are included in Figure 3. Around each square both straight (black cable) and helical-wound (blue cable) fibres were deployed, each cable wrapping twice about each square.

According to the least-squares scheme discussed by Innanen (2017a), to create robust and complete tensor strain (or strain-rate) estimates, a fibre must be shaped such that it has intervals in many different orientations, with each of the three coordinate directions represented. Furthermore, in order to say that a certain direction has been meaningfully

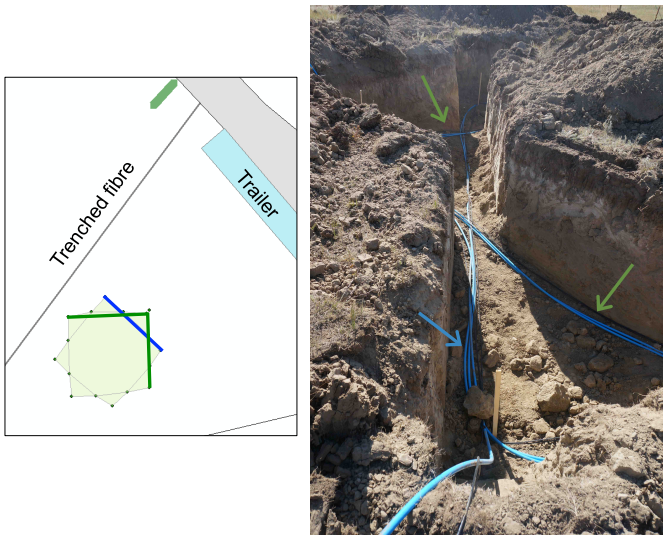

FIG. 3. Detail of the deployment and fibre configuration. Left: three segments of the array are highlighted in green and blue; right: photograph of the trench with the straight (black cable) and helical-wound (blue cable) fibres visible. Both cables were wound twice each around each square. All corners and crossover points' depths and lateral locations were surveyed with RTK-GPS and hand measured.

occupied by a fibre, it must run uninterrupted in that direction for a distance at least that of the interrogator gauge length. Currently, gauge lengths of no lower than order 5-10m should be assumed. Lower values may be often available, but dropping significantly below the 5-10m standard will tend to strongly impact signal-to-noise ratios. Two observations arise in light of these remarks:

1. Gauge length restrictions put a strong lower bound on the size of a multicomponent DAS "sensor" of the type contemplate: 5-10m intervals in each coordinate direction to be characterized are required. At this size the loop cannot be considered a point sensor of waves traveling at standard seismic velocities and frequencies.

2. The fibre loop sensor we deployed lacks vertical coverage. The fibre occupies vertical directions as it enters and leaves the trench, but these lengths are on the order of 2m; assuming a 5-10m gauge length, the vertical signal will be impure (though possibly usable).

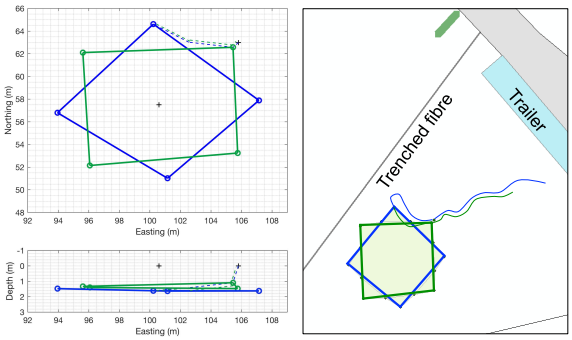

FIG. 4. Geometrical model of buried DAS fibre loop. Top left: map view; bottom left: easting vs. depth; right panel: blue and green square reference sketches.

All corner and crossover points of the fibre were surveyed with the RTK-GPS system for lateral position and depth; these measurements were also supplemented by tape-measure

readings, especially to confirm depth estimates. These GPS and hand-measured coordinates were then used to create a computer model of the fibre loop geometry (Figure 4).

SOURCE GEOMETRY

The array was illuminated by 10-150Hz sweeps from the University of Calgary Envirovibe at four different locations (see Figure 5); each sweep was repeated 10 times and stacked to maximize signal. The vibe points were surveyed and are illustrated relative to the buried loop in Figure 5.

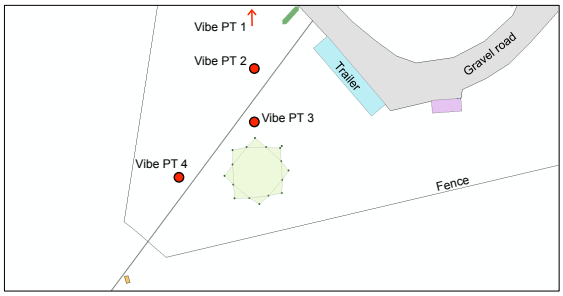

FIG. 5. Three of four approximate source points overlain on CaMI-FRS map with buried loop.

The middle-offset vibe point (VP2), about 30m from the centre of the fibre array, was selected for detailed first analysis, balancing as it does sufficient proximity to maximize signal strength with sufficient propagation distance to have body wave modes arrive distinctly.

SYNTHETICS

To quantify the signal we expected to be sensed by the buried DAS loop, simple synthetics were computed based on the assumption that the earlier arrivals at the fibre would be body waves carrying characteristic strains along simple ray paths.

Strain or strain rate and fibre geometry

Let the DAS fibre, sources, and all seismic rays be embedded in a volume as illustrated in Figure 6. The volume is defined within an orthogonal field coordinate system consisting of inline, crossline, and depth axes. The DAS response is modelled via a careful accounting of the fibre geometry in the volume. Here we will provide a brief outline; for a full discussion see Innanen (2017a) and Eaid and Innanen (2018).

A DAS fibre is assumed to describe a smooth curve within the volume; a local orthogonal coordinate system is defined based on the unit tangent $\hat{\mathbf{t}}$ of the fibre at all points along its arc-length s. The plane normal to $\hat{\mathbf{t}}$ is spanned by the two other unit vectors, which are referred to as the normal and binormal vectors, $\hat{\mathbf{n}}$ and $\hat{\mathbf{b}}$ respectively. The strain tensor e with components defined in this coordinate system will be called e_{tnb}. At any point along the fibre, seismic energy might arrive along a raypath which has a characteristic coordinate system of its own, also locally (for heterogeneous media) or globally (for homogeneous media) defined in terms of ray tangent and normal/binormal directions, which we will number

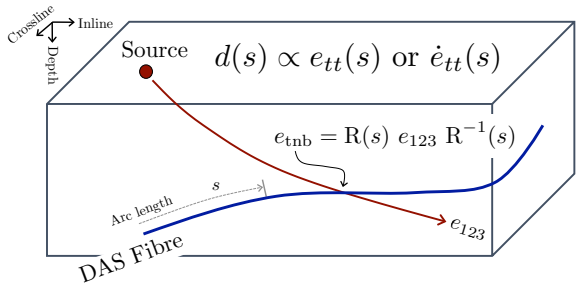

FIG. 6. Ray and DAS fibre geometries and their relationship determines the DAS response at any point along its arc-length.

$\hat{\mathbf{1}}$, $\hat{\mathbf{2}}$ and $\hat{\mathbf{3}}$, with $\hat{\mathbf{1}}$ being the tangent direction. A strain tensor e with components defined in this coordinate system will be called e_{123}.

The DAS fibre at the point s responds proportionally to the longitudinal strain (or strain-rate) projected onto the $\hat{\mathbf{t}}$ direction. If we define elastic strain being carried by a seismic wave as e_{123} in the ray coordinate system, when it arrives at s along the fibre at time t, the response can be directly read from the first (tt) component of the tensor

$$e_{tnb}(s,t) = \mathbf{R}(s) e_{123}(s,t) \mathbf{R}^{-1}(s), \tag{1}$$

where

$$\mathbf{R}(s) = \begin{bmatrix} \hat{\mathbf{t}}\cdot\hat{\mathbf{1}} & \hat{\mathbf{t}}\cdot\hat{\mathbf{2}} & \hat{\mathbf{t}}\cdot\hat{\mathbf{3}} \\ \hat{\mathbf{n}}\cdot\hat{\mathbf{1}} & \hat{\mathbf{n}}\cdot\hat{\mathbf{2}} & \hat{\mathbf{n}}\cdot\hat{\mathbf{3}} \\ \hat{\mathbf{b}}\cdot\hat{\mathbf{1}} & \hat{\mathbf{b}}\cdot\hat{\mathbf{2}} & \hat{\mathbf{b}}\cdot\hat{\mathbf{3}} \end{bmatrix}. \tag{2}$$

That is, if

$$e_{tnb} = \begin{bmatrix} e_{tt} & e_{tn} & e_{tb} \\ e_{nt} & e_{nn} & e_{nb} \\ e_{bt} & e_{bn} & e_{bb} \end{bmatrix}, \tag{3}$$

then $d(s,t) = e_{tt}(s,t)$; or, if the interrogator response is proportional to strain rate $d(s,t) = \dot{e}_{tt}(s,t)$. We incorporate gauge length by integrating this point strain definition over fibre intervals, normally with a Gaussian window. Each channel location thus represents a mean strain computed over half a gauge length on either side.

Shot records

The DAS data after vendor (in this case Halliburton) pre-processing is stored as shot records with traces separated by a constant channel spacing and characterized by a fixed gauge length (1.02m and 10m respectively in this experiment). DAS output is directly in terms of arc-length along the fibre, i.e., the distance associated with optical propagation times and the speed of light in glass. Therefore, all geometric aspects of the fibre loop we deployed must be brought into consideration after the fact: the horizontal axis of the shot record is an "unwrapped" version of the fibre segments we have been considering so far. See Figure 7.

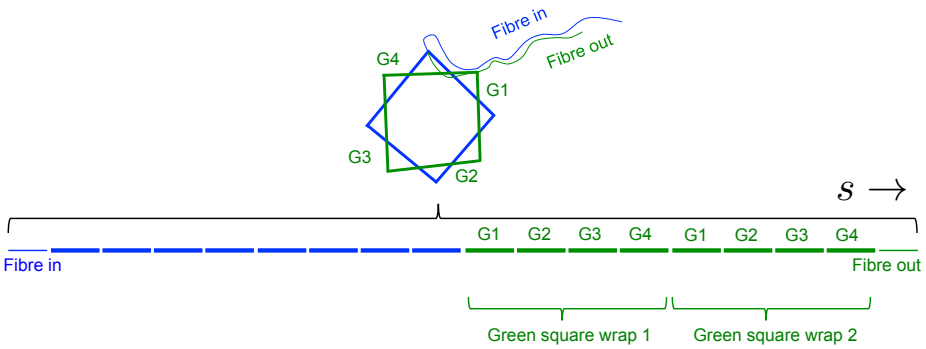

FIG. 7. Fibre shape and its appearance when "unwrapped" (with segments associated with the edges of the green square labelled as an example). The linear unwrapped fibre length at the bottom matches the horizontal axis of shot records generated from interrogator measurements.

Choosing a causal wavelet and assuming a P-wave with first strain positive in the direction of propagation, propagating in a homogeneous medium velocity V_P=500m/s, the shot record in Figure 8 is produced. Overlain on the figure is the schematic diagram of the unwrapped fibre.

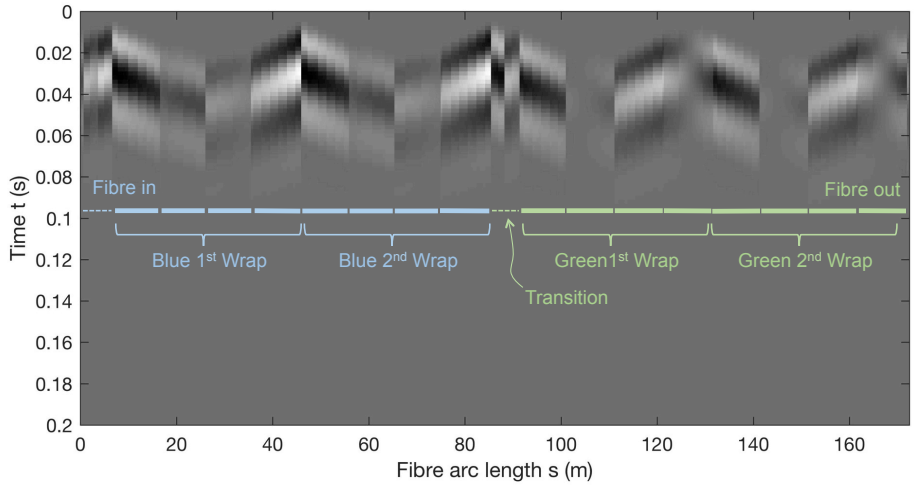

FIG. 8. Synthetic shot record on DAS fibre loop with field geometry. Overlain is the unwrapped fibre loop with each segment labelled.

We observe that with the P-wave moving slowly in the near surface, and at standard seismic frequencies, the loop will respond as a point sensor; specifically, approximately piece-wise linear moveout should be expected across the length of the fibre. If lower frequency waveforms are used, or if the signal is filtered to pass only wavelengths much greater than the 10m scale of the loop, this pattern will diminish.

Directionality

The amplitudes in the synthetic responses (e.g., the shot record in Figure 8) are dominated by the directionality of the fibre. Geometric spreading is a second order influence, difficult to see in these plots, but when we look more closely at the synthetics its influence will become apparent also.

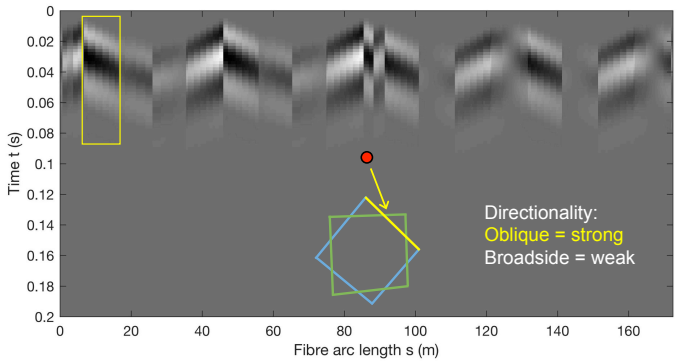

FIG. 9. Shot record with response from one segment of the square highlighted. Here the strain delivered by the P-wave was aligned with the fibre and the amplitude is consequently relatively high.

To put the amplitude variations into their geometric context, consider two parts of the shot record. In Figure 9, a yellow box is drawn around the response from one of the edges of the blue square in the loop; the associated edge is indicated in yellow also. Notice that if a P-wave is incident on this segment from the red source point (i.e., from VP2), then the ray intersects the fibre obliquely, and thus its strain, which is longitudinal and aligned with the ray, will be largely aligned with the fibre, producing a high-amplitude response.

In contrast, in Figure 10, the ray carries the longitudinal strain of the P-wave across a segment of the fibre to which it is almost perpendicular. This is the direction of the lowest sensitivity of the fibre and so the response (again indicated with a yellow box) is almost zero.

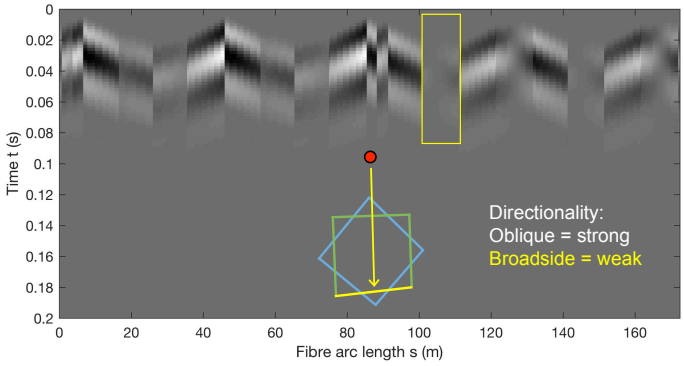

FIG. 10. Shot record with response from one segment of the square highlighted. Here the strain delivered by the P-wave was almost perpendicular to the fibre and the amplitude is consequently relatively low, in fact almost zero.

Polarity

In addition to the weak versus strong amplitude responses arising from the projection of the strain onto fibre elements going in a range of directions, clear polarity reversals appear in the raw application of the CREWES geometrical model, by virtue of the tangent vector $\hat{\mathbf{t}}$, which is locally parallel to the fibre and by design oriented away from the interrogator. Accounting for geometry in this way, if two antiparallel segments of the fibre see the same strain, one will register it as positive and the other as negative. This is visible in

the synthetic shot record. See Figures 11-12, and bear in mind that the sense of the fibre is clockwise. In Figure 11, the response of a segment of the fibre whose tangent opposes the ray direction (and which therefore is negative) is highlighted. In Figure 12, the segment in contrast aligns with the ray direction, and the fibre response is therefore predicted to be positive.

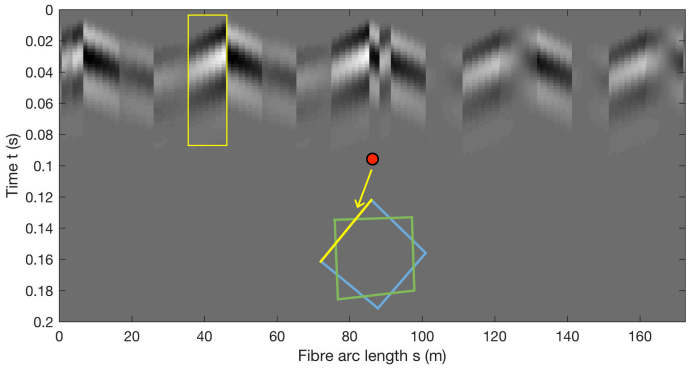

FIG. 11. Shot record amplitude response for a segment of the DAS fibre whose tangent opposes the ray direction.

This predicted polarity reversal is a natural result of the differential geometry used to characterize the fibre shape. It is a reflection of what it means "to project" the seismic strain onto a directed curve. However, it is not necessarily what a DAS fibre will register; in fact a simple accounting for the manner in which strain is sensed by a fibre suggests that the *sense* of the fibre should not have any influence on what is measured.

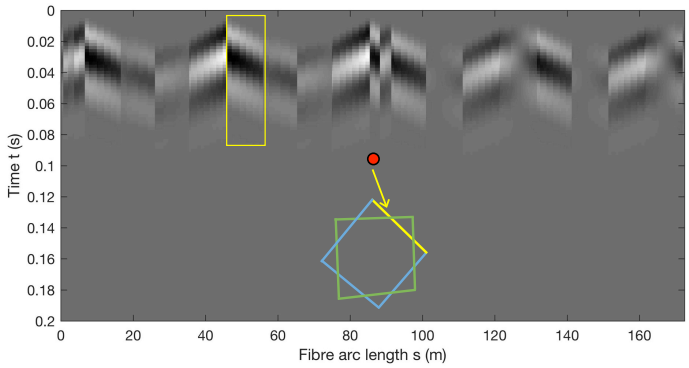

FIG. 12. Shot record amplitude response for a segment of the DAS fibre whose tangent aligns with the ray direction.

Let us set up a simple conceptual picture in order to argue that the polarity reversals used by the geometrical model will not appear, at least for certain interrogators, in the data, and that to accurately use the former to discuss the latter correction should be employed. In Figure 13 a segment of a fibre that bends back on itself is sketched. Channel points on the fibre are labelled with position numbers which grow in proportion to arc-length. Let us suppose that this loop is sufficiently small that any point along the top segment (e.g., 5) will experience the same strain as its counterpart along the bottom segment (e.g., 28). Then let us specify an example distortion. Consider fibre points 5 and 6 on the top segment, which are coloured blue and red respectively. The numbers 5 and 6 are replaced by two additional labels, B_1 and B_2, with B meaning "before" the strain, to make things explicit. Then, let

us proceed along the fibre in the direction of growing arc-length, until we come around the loop and arrive back to the same region of space. Label the two counterpart points, 28 and 29, B_3 and B_4, with the rightmost coloured red and the leftmost coloured blue.

Now, if the region with the B labels experiences a constant seismic strain, does the top part of the segment see a polarity-reversal relative to the bottom by virtue of the change in fibre direction?

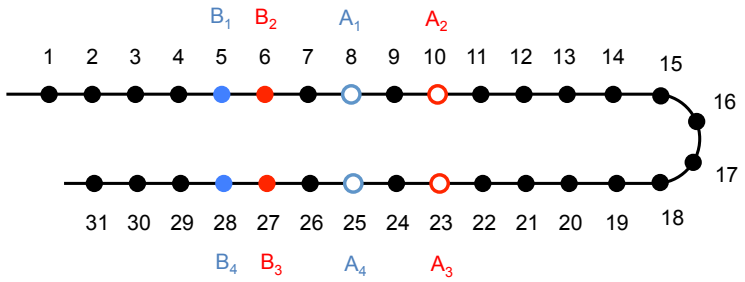

FIG. 13. Schematic illustration of a segment of fibre looping back on itself. If this loop experiences an axial strain, does the upper leg of the fibre see a polarity reversed version of what the lower leg sees?

Suppose the four B (solid coloured) points on the fibre are distorted by the strain of a passing seismic wave. The area around the B points will have experienced strain if the displacements of the blue dots are different from the displacement of the red dots. Let B_1 be displaced to A_1 (where A means "after" the strain) and B_2 be displaced to A_2. These are illustrated as open circles in the Figure. Calling the displacement of point 1 u_1, and the displacement of point 2 u_2, we have (in units of channel number)

$$\begin{aligned} u_1 &= A_1 - B_1 = 8 - 5 = 3, \\ u_2 &= A_2 - B_2 = 10 - 6 = 4. \end{aligned} \tag{4}$$

Because the fibre loop is small, B_3 and B_4 experience the same distortion as B_1 and B_2 did, which means that B_4 is displaced to A_4 and B_3 to A_3:

$$\begin{aligned} u_3 &= A_3 - B_3 = 23 - 27 = -4, \\ u_4 &= A_4 - B_4 = 25 - 28 = -3. \end{aligned} \tag{5}$$

The longitudinal strain on the high side of the fibre will be measured as

$$e_H \approx \frac{u_2 - u_1}{B_2 - B_1} = \frac{4-3}{6-5} = 1, \tag{6}$$

and on the low side as

$$e_L \approx \frac{u_4 - u_3}{B_4 - B_3} = \frac{-3-(-4)}{28-27} = 1. \tag{7}$$

No polarity-reversal is to be expected.

In summary, the CREWES geometrical model of DAS response assigns a polarity to the strain at each point or gauge interval on the fibre, which will reverse itself if the direction

of the fibre (or a relevant component of it) reverse direction. The polarity is a consequence of the sense of the fibre, which is communicated to the directionality calculation via the tangent vector. However, a simple conceptual picture of the way fibre impurities and their relative positions will be analyzed for strain estimates is suggestive that many interrogators will not assign such polarities to the responses.

The polarity in the geometrical model is convenient to maintain, but this discussion emphasizes the fact that it will not tend to match what is seen in DAS data. This can be easily remedied in modelling or in data analysis, by either suppressing the polarity in the analytical model or adding it to the data. To add or suppress the polarity, if the component of $\hat{\mathbf{t}}$ aligned with the source-fibre unit vector is positive/negative, we multiply the modeled or the measured axial strain estimate by +1/-1. In the following, we will alter the data as a pre-processing step.

FIELD DATA

The stacked (10 sweeps) shot record from the source at VP2 is plotted in Figure 14. Overlain are two event interpretations, and a label emphasizing the lack of polarity reversals as discussed above. The synthetics we devised were built for P-wave arrivals on the assumption that the first-arrival amplitudes would be the easiest to evaluate for directivity. The moveout patterns are suggestive that a P arrival is first, followed by S-wave energy which may immediately, and if not immediately then very soon after, also contain surface wave energy.

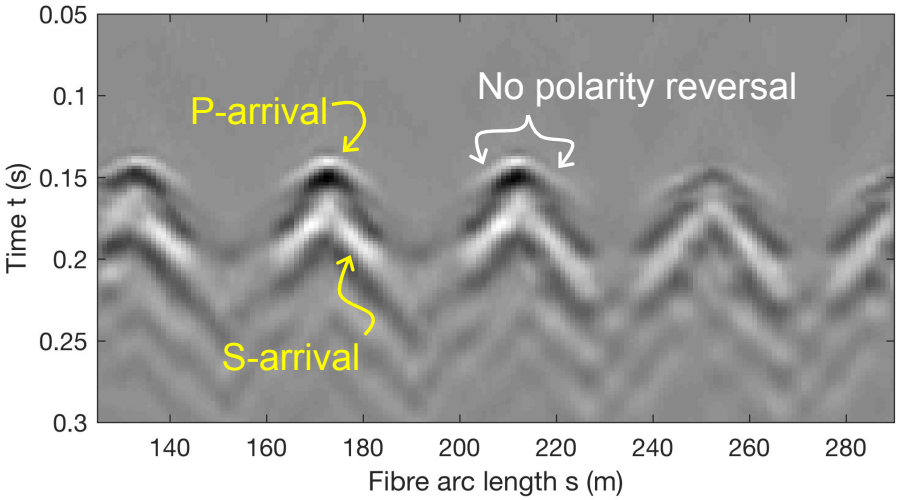

FIG. 14. Shot records produced by the Halliburton interrogator from the stacking of 10 sweeps at VP2. Two event interpretations are overlain, as is a point of emphasis regarding polarity.

The directivity patterns predicted in the synthetics are largely present in the field data. This is the primary conclusion of our experiment (compare Figures 8 and 14): that the basic elements of multicomponent sensing are present. The leftmost three "rooftop" arrivals are bright at their apexes, dimming elsewhere; the leftmost legs have even dimmer "valley" responses; the transition between the blue and the green squares, occurring past 80m into

the loop on the synthetic and past 200m on the field data* is particularly visible in the field data in the later arrivals into the fibre.

Processing

Some simple processing was carried out to quantitatively assess the match between the analytic data and the measured data. We emphasize that most of this processing (except for the moveout correction) is only to allow the assessment to take place, and would not be required if the raw data were being used directly for multicomponent estimation.

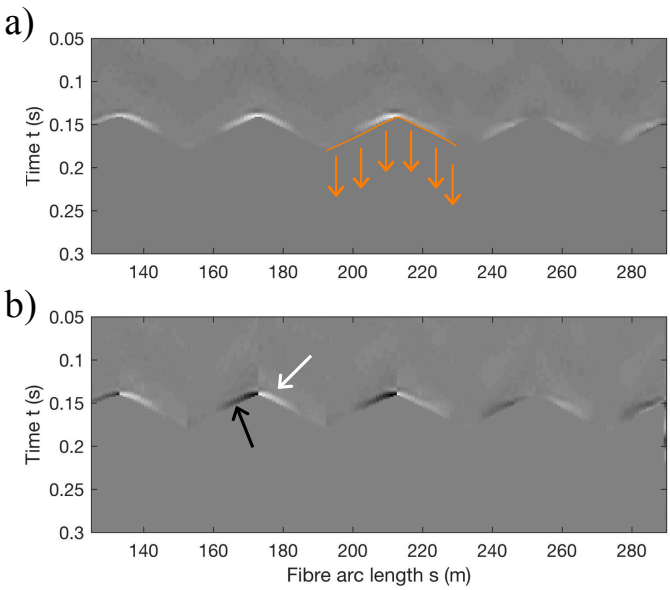

FIG. 15. Processing. (a) Muting below the first arrivals; (b) adding geometric polarity (arrows).

First, to accentuate the P-wave arrival (whose strain is included in the analytic modelling), a mute after the first arrival was applied (Figure 15a). Second, in order to permit a comparison with the analytic data, which (as discussed in the previous section) adds a polarity change based on the relative directions of the fibre tangent vector and the ray vector, the known source and fibre geometry was used to add this polarity change in to the field data as well.

The next issue is a slightly complex one, in light of our eventual aim to make treat DAS arrays like this as multicomponent sensors. The size of the loop, roughly 10×10m, was decided on based on gauge length considerations. A complication of these choices is that a seismic wave will not see this loop, even approximately, as a point sensor. This is clear in the moveout patterns in the synthetics and real data: in our experiment the gauge-length compliant loop cannot be considered a point sensor.

This can be corrected for (or managed) in one of several ways. First, by treating the

*On the field data, the loop begins at roughly 120m along the fibre, while in the synthetics we have set arc-length to zero at the beginning of the loop; to compare the field data to the synthetic, subtract 120m from the horizontal axis on the field record.

loop as a sensor for low-frequencies only. The dominant frequency of the P-wave arrival in Figures 14-15 is close to 100Hz; if the P-wave is travelling at $n\times$100m/s, its dominant wavelength will therefore be roughly n metres. To appear as a point sensor to such a wave, our loop would have to be several times smaller than this. Evidently the wave velocity must exceed 1000m/s by several times for this to be true, which is unrealistic, especially in the near surface. However, at 10Hz, waves moving at $n\times$100m/s have wavelengths on the order of $10\times n$ metres, which is much larger than the sensor footprint for most realistic velocities. So, the loop we buried can be treated as a point sensor for wave data filtered to pass frequencies near 10Hz but not those near 100Hz.

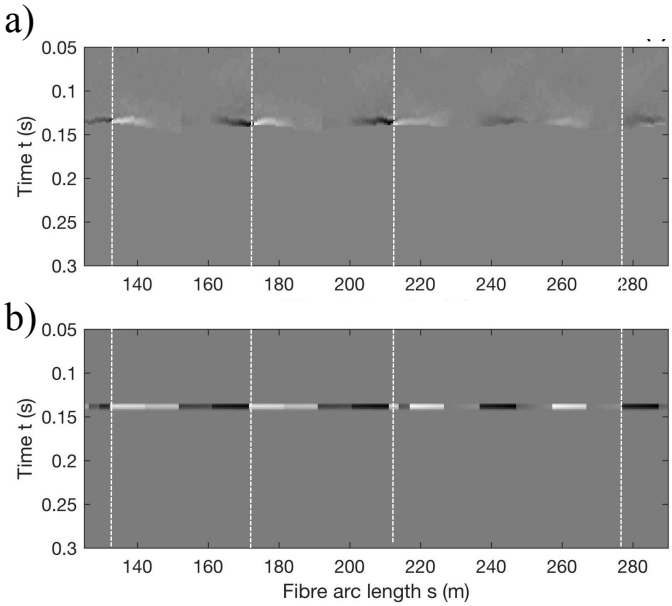

FIG. 16. Processed first breaks. (a) Field data; (b) synthetics. The reference white dashed lines provide some sense of the match between synthetic and measured data.

Another partial solution is to accept that the loop is not a point sensor, and define some internal processing to correct for its spatial distribution. Since we are focusing on a single mode P-wave arrival, this is much the most straightforward approach and we adopt it here. We determine flattening velocities for the moveout patterns observed along the distinct segments of the fibre loop, and carry out a moveout correction. After the correction, the amplitudes in a time slice through the muted/polarity-altered data approximate the strains carried by the same point on the P-wave wavefront, projected in a range of different directions. In Figure 16a, the corrected field data are plotted; the first amplitudes of the synthetic with the moveout removed is plotted in comparison in Figure 16b.

Analysis of a time-slice through the array

Let us focus on a time slice through the arriving P-wave so a more complete comparison can be made between the measured and the predicted amplitudes and directivity patterns. In Figure 17a, the raw measured amplitudes are plotted in black, and the raw predicted amplitudes are plotted in red. Consider the red synthetic amplitudes first. The discontinuities represent the sudden changes in direction of the DAS fibre; within each segment the average amplitudes primarily reflect the directional sensitivity of the fibre segments to the

incoming wave strain. Also within each segment a progressive dimming or brightening is visible; this is the geometrical spreading caused by variation in propagation distance between the source and each point on the fibre. The complex transition between the blue and green squares, between 205m and 220m is zeroed out in these data.

Although the absolute amplitudes between the field and synthetic data do not precisely match, both the first order directionality trends in the amplitudes, and the second order geometrical spreading trends, are apparent in the field data. This is a key observation of this paper.

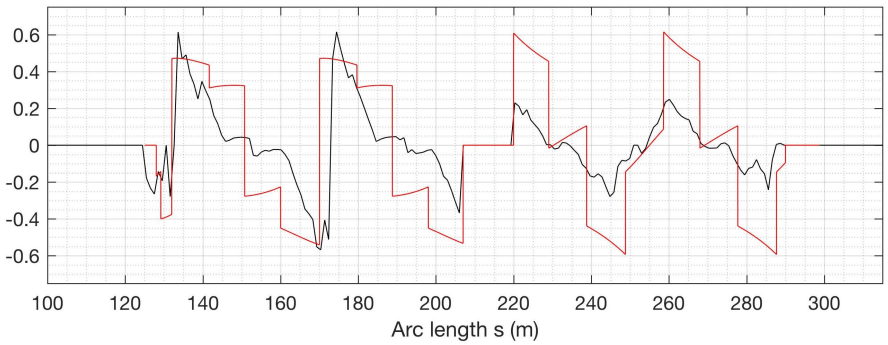

FIG. 17. Amplitudes in the time-slice through the shot record: field data (black) versus synthetic (red).

MULTICOMPONENT STRAIN ESTIMATION

Innanen (2017a) presented a formula with which to estimate the 6 independent components of tensor strain within DAS fibre reconstruction windows, assuming the presence of fibre intervals spanning all three spatial coordinate directions. In this section we examine the use of that formulation to carry out multicomponent sensing with the buried array.

Conditioning and depth coverage

Let the right handed coordinate system involving the directions west, north, and depth be labelled W, N and D respectively. A strain tensor evaluated in this coordinate system would have components

$$\mathbf{e} = \begin{bmatrix} e_{WW} & e_{WN} & e_{WD} \\ \cdot & e_{NN} & e_{ND} \\ \cdot & \cdot & e_{DD} \end{bmatrix}. \tag{8}$$

A forward modelling formula for M measurements of axial strain $e_{tt}(s_i)$, i=(1,M), assuming the fibre to be embedded in a volume in which the strain is constant and described by the tensor in equation (10), is

$$\begin{bmatrix} e_{tt}(s_1) \\ e_{tt}(s_2) \\ \vdots \\ e_{tt}(s_M) \end{bmatrix} = \mathbf{L} \begin{bmatrix} e_{WW} \\ e_{WN} \\ e_{WD} \\ e_{NN} \\ e_{ND} \\ e_{DD} \end{bmatrix}, \tag{9}$$

where

$$\mathbf{L} = \begin{bmatrix} \lambda^1_{WW} & 2\lambda^1_{WN} & 2\lambda^1_{WD} & \lambda^1_{NN} & 2\lambda^1_{ND} & \lambda^1_{DD} \\ \lambda^2_{WW} & 2\lambda^2_{WN} & 2\lambda^2_{WD} & \lambda^2_{NN} & 2\lambda^2_{ND} & \lambda^2_{DD} \\ & & \vdots & & & \\ \lambda^M_{WW} & 2\lambda^M_{WN} & 2\lambda^M_{WD} & \lambda^M_{NN} & 2\lambda^M_{ND} & \lambda^M_{DD} \end{bmatrix}, \tag{10}$$

and

$$\lambda^k_{ij} = \left(\hat{\mathbf{t}}(s_k) \cdot \hat{\mathbf{i}} \right) \left(\hat{\mathbf{t}}(s_k) \cdot \hat{\mathbf{j}} \right), \tag{11}$$

with i and j ranging over W, N and D values. The directions explored by the shaped fibre are contained in the tangents in equation (11). Finally, assuming noise is present, a damped least-squares solution may be formed:

$$\begin{bmatrix} e_{WW} \\ e_{WN} \\ e_{WD} \\ e_{NN} \\ e_{ND} \\ e_{DD} \end{bmatrix} \approx \left(\mathbf{L}^T\mathbf{L} + \alpha\mathbf{I} \right)^{-1} \mathbf{L}^T \begin{bmatrix} e_{tt}(s_1) \\ e_{tt}(s_2) \\ \vdots \\ e_{tt}(s_N) \end{bmatrix}. \tag{12}$$

The issue at hand is that the prototype sensor we deployed has no coverage in the depth direction. Consequently, the version of $\mathbf{L}$ associated with the geometry of our loop will be severely rank-deficient, and $\mathbf{L}^T\mathbf{L}$ will have no inverse.

This leads to two separate concerns. First, how to stably proceed to determine those components of the tensor which *are* constrained by our data; and second, whether determining some but not all of the strain tensor components is of any direct value. The first issue is straightforwardly solved (in fact, the α takes care of the issue). The second we will not worry too much about in this paper. The purpose here is to see whether with currently available DAS technology multicomponent sensing is feasible. Finding this out for a restricted set of strain components is enough to answer our pressing feasibility questions.

The parameter α in principle corrects for the issue of missing rank, both accounting for noise and allowing the 3 components of the tensor constrained by the data to be estimated. To simplify matters, however, we will explicitly remove the 3 components of e not constrained by our experiment (e_{WD}, e_{ND} and e_{DD}), producing a reduced version of the system:

$$\begin{bmatrix} e_{WW} \\ e_{WN} \\ e_{NN} \end{bmatrix} \approx \left(\mathbf{L}_r^T\mathbf{L}_r + \alpha\mathbf{I} \right)^{-1} \mathbf{L}_r^T \begin{bmatrix} e_{tt}(s_1) \\ e_{tt}(s_2) \\ \vdots \\ e_{tt}(s_N) \end{bmatrix}, \tag{13}$$

where

$$\mathbf{L}_r = \begin{bmatrix} \lambda^1_{WW} & 2\lambda^1_{WN} & \lambda^1_{NN} \\ \lambda^2_{WW} & 2\lambda^2_{WN} & \lambda^2_{NN} \\ & \vdots & \\ \lambda^M_{WW} & 2\lambda^M_{WN} & \lambda^M_{NN} \end{bmatrix}; \tag{14}$$

here the parameter α can be used to focus on noise. Given the fibre loop geometry discussed in the previous sections, we can expect the system $\mathbf{L}_r^T\mathbf{L}_r + \alpha\mathbf{I}$ in equation (13) to have a stable inverse. In fact the independent directions of two squares at 45° to one another produce the basic matrix

$$\mathbf{L}_r = \begin{bmatrix} 1/2 & 1 & 1/2 \\ 1/2 & -1 & 1/2 \\ 1 & 0 & 0 \\ 0 & 0 & 1 \end{bmatrix}, \tag{15}$$

such that

$$\mathbf{L}_r^T\mathbf{L}_r = \begin{bmatrix} 3/2 & 0 & 1/2 \\ 0 & 2 & 0 \\ 1/2 & 0 & 1/2 \end{bmatrix} \tag{16}$$

has the well-behaved inverse

$$\left(\mathbf{L}_r^T\mathbf{L}_r\right)^{-1} = \begin{bmatrix} 3/4 & 0 & -1/4 \\ 0 & 1/2 & 0 \\ -1/4 & 0 & 3/4 \end{bmatrix}. \tag{17}$$

Synthetic and field estimates

The instantaneous profiles plotted in Figure 17 permit us to carry out an estimation of the instantaneous components of strain excluding depth. Correcting for geometrical spreading, and averaging within the segments (which will introduce error into the estimate), we can assign approximate values to each of the directions used to form the matrix $\mathbf{L}_r$ in the previous section, after which we may use equation (17) to determine the three components in the W-N-D coordinate system. In the synthetic case, in which a pure P-wave travelling from the north was assumed, the "right answer" is

$$\mathbf{e} = \begin{bmatrix} e_{WW} & e_{WN} & e_{WD} \\ \cdot & e_{NN} & e_{ND} \\ \cdot & \cdot & e_{DD} \end{bmatrix} = \begin{bmatrix} 0 & 0 & e_{WD} \\ \cdot & 1 & e_{ND} \\ \cdot & \cdot & e_{DD} \end{bmatrix}. \tag{18}$$

This is more or less captured in the synthetic data:

$$\mathbf{e}_{\text{synth}} = \begin{bmatrix} 0.13 & 0.03 & e_{WD} \\ \cdot & 0.74 & e_{ND} \\ \cdot & \cdot & e_{DD} \end{bmatrix}; \tag{19}$$

the leakage of P-wave strain into the NW and WW components is a measure of the error introduced by using a bulk average across the segments. As the ray crosses segments of constant direction, the actual strain projected onto the fibre changes, and by averaging we neglect these variations. This is an unavoidable result of large gauge-lengths on multicomponent sensing. The field data have patterns on the second square which do not match our synthesized P-wave, so we should not expect to see the strain estimate recreating equation

(18). The loop is seeing a significantly dimmer response on the second loop than on the first. There is no reason to expect that coupling in one part of the backfilled trench will be so regularly different from that of another part (and there are parts of these loops that lie very close to one another and must have essentially identical coupling properties). We conclude that the response seen by the fibre loop is real, and reflects not a problem with the sensing but rather a deviation of the elastic distortion on the fibre away from the assumed pure P-wave. The strain we estimate is

$$\mathbf{e}_{\text{field}} = \begin{bmatrix} 0.04 & 0.11 & e_{WD} \\ \cdot & 0.26 & e_{ND} \\ \cdot & \cdot & e_{DD} \end{bmatrix}; \tag{20}$$

i.e., much of the strain component distribution of a P-wave coming from the north, but with nonnegligible energy which must be ascribed to one or more other modes.

CONCLUSIONS

In 2016-2017 CREWES published a range of analyses and applications of a geometrical model of fibre-optic (DAS) data for arbitrary fibre shapes. Amongst those applications was a multicomponent estimation scheme based on a careful accounting, and combined useage, of the varying fibre directions associated with a shaped cable layout. In 2018 a prototype shaped DAS fibre array was buried to put some of these ideas and their feasibility to the test. In October 2018, "the pretzel" was illuminated from several directions, and shot records were analyzed to assess whether commonly available directional sensitivity is sufficient to permit multiple components of strain to be estimated simultaneously. By picking a P-wave arrival and comparing it to an analytic model, we conclude with a cautious yes. Other important directionality conclusions are also derivable from this experimental setup; for instance, a polarity ambiguity involving the DAS directionality modelling through accounting of local fibre tangents is clearly rendered when model and data are compared.

ACKNOWLEDGEMENTS

We thank the sponsors of CREWES for continued support. This work was funded by CREWES industrial sponsors, NSERC (Natural Science and Engineering Research Council of Canada) through the grant CRDPJ 461179-13, and in part thanks to the Canada First Research Excellence Fund. Halliburton is gratefully acknowledged for deploying their interrogator for the field testing; CaMI for supporting the array deployment on its FRS; and Lawrence Berkeley National Labs for supplying the helical wound cable used in the loop.

REFERENCES

Chalenski, D., Tatanova, M., Du, Y., Lopez, J., Mateeva, A., and Potters, H., 2016, Climbing the staircase of ultra-low cost 4D monitoring of deepwater fields using DAS-VSP: SEG Expanded Abstracts.

Daley, T. M., Freifeld, B. M., Ajo-Franklin, J., Dou, S., Pevzner, R., Shulakova, V., Kashikar, S., Miller, D. E., Goetz, J., Henninges, J., and Lueth, S., 2013, Field testing of fiber-optic distributed acoustic sensing (DAS) for subsurface seismic monitoring: The Leading Edge, **32**, No. 6.

Eaid, M., and Innanen, K. A., 2018, Modeling the sensitivity of shaped das fibre-optic cables to elastic wave data: CSEG Expanded Abstracts.

Eaid, M., Li, J., and Innanen, K. A., 2018, Modeling the response of shaped das fibres to microseismic moment tensor sources: SEG Expanded Abstracts, 4698–4702.

Hall, K. W., Bertram, K. L., Bertram, M., Innanen, K. A., and Lawton, D. C., 2018, Crewes 2018 multi-azimuth walk-away vsp field experiment: CREWES Annual Report, **30**.

Hall, K. W., Lawton, D. C., Daley, T., Freifeld, B., and Cook, P., 2017, Source distance and source effort on das data: CREWES Annual Report, **29**.

Hardeman-Vooys, H. K., Li, D., Cova, R., and McDonald, M., 2018, Phase unwrapping methods applied to distributed acoustic sensing data: CREWES Annual Report, **30**.

Huot, F., Martin, E. R., and Biondi, B., 2018, Automated ambient-noise processing applied to fiber-optic seismic acquisition (das): SEG Expanded Abstracts, 4688–4692.

Innanen, K. A., 2016, A geometrical model of das fibre response: CREWES Annual Report, **28**.

Innanen, K. A., 2017a, Determination of seismic tensor strain from hwc-das cable with arbitrary and nested-helix winds: SEG Expanded Abstracts.

Innanen, K. A., 2017b, Parameterization of a helical DAS fibre wound about an arbitrarily curved cable axis: EAGE Expanded Abstracts.

Kuvshinov, B. N., 2016, Interaction of helically wound fibre-optic cables with plane seismic waves: Geophysical Prospecting, **64**, 671–688.

Mateeva, A., Lopez, J., Mestayer, J., Wills, P., Cox, B., Kiyashchenko, D., Yang, Z., Berlang, W., Detomo, R., and Grandi, S., 2013, Distributed Acoustic Sensing (DAS) for reservoir monitoring with VSP: The Leading Edge, **32**, 1278–1283.

Mateeva, A., Lopez, J., Potters, H., Mestayer, J., Cox, B., Kiyashchenko, D., Wills, P., Grandi, S., Hornman, K., Kuvshinov, B., Berlang, W., Yang, Z., and Detomo, R., 2014, Distributed acoustic sensing for reservoir monitoring with vertical seismic profiling: Geop. Prosp., **62**, 679–692.

Mestayer, J., Cox, B., Wills, P., Kiyashchenko, D., Lopez, J., Costello, M., Bourne, S., Ugueto, G., Lupton, R., Solano, G., Hill, D., and Lewis, A., 2011, Field trials of distributed acoustic sensing for geophysical monitoring: SEG Expanded Abstracts.

Ning, I. L. C., and Sava, P., 2018, Multicomponent distributed acoustic sensing: concept and theory: Geophysics, **83**, No. 2, P1–P8.

Willis, M. E., Ellmauthaler, A., LeBlanc, M., Palacios, W., and Wu, X., 2018, Comparing distributed acoustic sensing, vertical seismic profile data acquired with single- and multi-mode fiber optic cables: SEG Expanded Abstracts, 4674–4678.

Yu, G., Sun, Q., Ai, F., Yan, Z., Li, H., and Li, F., 2018, Microstructured fiber distributed acoustic sensing system for borehole seismic survey: SEG Expanded Abstracts, 4669–4673.